

Calculating Quantum Transports Using Periodic Boundary Conditions

Lin-Wang Wang

*Computational Research Division, Lawrence
Berkeley National Laboratory, Berkeley, CA 94720*

(Dated: November 23, 2018)

Abstract

An efficient new method is presented to calculate the quantum transports using periodic boundary conditions. This new method is based on a method we developed previously, but with an essential change in solving the Schrodinger's equation. As a result of this change, the scattering states can be solved at any given energy. Compared to the previous method, the current method is faster and numerically more stable. The total computational time of the current method is similar to a conventional ground state calculation. Details of the procedure is presented in the current paper.

PACS numbers: 71.15.-m, 73.63.-b, 73.22.-f

I. INTRODUCTION

Molecular elastic quantum transport has been studied intensely in recent years both in theory and experiment[1, 2, 3, 4, 5, 6, 7]. Theoretically, the total current through a molecule connected by two electrodes can be calculated as:

$$I = \frac{2e}{h} \int_{\mu_L}^{\mu_R} \sum_n T_n(E) dE, \quad (1)$$

where μ_L and μ_R are left and right electrode Fermi energies (assuming the current flows from right to left in z direction), and $T_n(E)$ is the transmission coefficient for the n th right hand electrode band at energy E . One common way to calculate $T_n(E)$ is to calculate the scattering states $\psi_{sc}(r)$ at energy E which satisfies the Schrodinger's equation:

$$H\psi_{sc}(r) = E\psi_{sc}(r) \quad (2)$$

while having the following boundary conditions:

$$\psi_{sc}(r) = \begin{cases} \phi_m^{R*}(r) + \sum_{n \neq m} B_n^R \phi_n^R(r) & \text{if } z \rightarrow \infty \\ \sum_n A_n^L \phi_n^{L*}(r) & \text{if } z \rightarrow -\infty \end{cases} \quad (3)$$

Note that, in Eq(2), $H = \{-\frac{1}{2}\nabla^2 + V(r) + V_{nonloc}\}$ is the single particle Hamiltonian. In Eq(3), $\phi_n^{R(L)}(r) = u_{n,k_n}(r) \exp(ik_n^{R(L)}z)$, are the right going running waves in the the right(R) and left(L) electrodes, and $\phi_n^{R(L)*}$ are the left going running waves. $E_n^{R(L)}(k_n^{R(L)}) = E$ are the electrode band structure. The summation \sum_n in Eq(3) stands for all band n and $k_n^{R(L)}$ which satisfy $E_n^{R(L)}(k_n^{R(L)}) = E$. In Eq(3), we have assumed that $dE_n^{R(L)}(k)/dk > 0$ for band n . If one band n has $dE_n^{R(L)}(k)/dk < 0$, then its corresponding $\phi_n^{R(L)}(r)$ in Eq(3) should be replaced by $\phi_n^{R(L)*}(r)$ for that particular band. Eq(3) describes an incoming running wave $\phi_m^{R*}(r)$ from the right electrode band m which is scattered back through outgoing running waves $B_n^R \phi_n^R(r)$ at the right electrode, and transmitted into the left going running waves $A_n^L \phi_n^{L*}(r)$ at the left electrode. As a result of this scattering process, the transmission coefficient for channel m can be calculated as

$$T_m(E) = \left[\sum_n |A_n^L|^2 (dE_n^L(k)/dk)|_{k=k_n^L} \right] / (dE_m^R(k)/dk)|_{k=k_m^R}. \quad (4)$$

Note that, due to current conservation, we have:

$$\sum_n |A_n^L|^2 (dE_n^L(k)/dk)|_{k=k_n^L} + \sum_{n \neq m} |B_n^R|^2 (dE_n^R(k)/dk)|_{k=k_n^R} = (dE_m^R(k)/dk)|_{k=k_m^R}. \quad (5)$$

Normally, Eqs(2),(3) are solved by using transfer matrix method [2, 3] or Lippmann-Schwinger equation [5]. However, transfer matrix method could be unstable in a multi-channel electrode [4] and it is difficult to deal with the nonlocal pseudopotential[3], and the application of Lippmann-Schwinger equation is computationally expensive[5].

In a previous publication [8], we have described a new method to calculate Eqs(2),(3) which uses a supercell with periodic boundary conditions, just like in a conventional ground state total energy calculation. In that method, a supercell eigenstates are solved using conventional conjugate gradient methods [9]. Then perturbations at one end of the electrode are introduced, and the eigenstates are recalculated using the same conjugate gradient method [9]. Next, these eigenstates are linearly recombined to make it satisfy the boundary condition Eq.(3). Although highly efficient compared to methods before it, and simple to implement since it uses only conventional ground state codes, that method has a drawback. In that method, the energy E in Eq(2) can only be the eigen energies of the original supercell Hamiltonian H . As a result, $T_n(E)$ is only known for a finite number of E (or say k_n). To overcome this problem, one needs to fit $T_n(k_n)$ with a continuous function before it is used to calculate the total current in Eq(1). Although it has been shown in Ref. 8 that this fitting over the k_n points is equivalent to the k-point summation in a supercell ground state calculation and it works fine in the case considered, but there might be cases where denser energy E points are needed, for example, close to a weakly coupled resonant tunneling. In this paper, we will provide an essential modification over our previous method. Under this new method, Eqs(2),(3) can be solved for arbitrary E , and the overall computation is faster than the previous method for much denser E point grid. We also provide details of the whole procedure in the current paper.

II. THE FORMALISM

In order to compare with our previous method in Ref. 8, we choose the same system as studied in that paper. The system is schematically shown in Fig.1 taken from Ref. 8. In the system, a benzene molecule is connected by two Cu quantum wires through the bonds of two

sulfur atoms. In Fig.1, left hand side B and right hand side B are periodically connected. As in Ref. 8, we will do nonselfconsistent calculations for finite bias, although selfconsistent calculation is straight forward using the scattering state solutions of Eqs(2),(3). To get the potential of a finite V bias system, self-consistent local density approximation (LDA) ground state calculation is performed for the zero bias system. Then, an additional smooth function is added to the potential to raise the right hand electrode by $V/2$ and lower the left hand electrode by $-V/2$. Norm conserving pseudopotentials are used, so is a planewave basis set with a 30 Ryd cutoff.

With some minor changes of notations, the essential idea of Ref. 8 [its Eq(6)] can be recast as to solve the wavefunction $\psi_{(l)}(r)$:

$$(H - E)\psi_{(l)}(r) = W_{(l)}(r), \quad (6)$$

here $W_{(l)}(r)$ are some perturbation functions which are only nonzero away from the molecule as shown in Fig.1. Note that, $\psi_{(l)}(r)$ has a supercell k-point \mathbf{K}_z , thus $u_{(l)}(r) = \psi_{(l)}(r)\exp(-i\mathbf{K}_z z)$ is periodic. \mathbf{K}_z could be, for example $\pi/2L_z$ where L_z is the supercell length in the z direction. After a few $\psi_{(l)}(r)$ are solved for a same energy E , these $\psi_{(l)}(r)$ can be linearly recombined with proper coefficients to generate a scattering state $\psi_{sc}(r)$ which satisfies the boundary conditions of Eq(3). In Ref. 8, Eq(6) is obtained by combining two eigen state equations with two different W_m [Eq(6) in Ref. 8]. Its advantage is that it needs only conventional eigen state calculations, thus there is no need to change a ground state code. The disadvantage, however, is that the energy E in Eq(6) can only be the eigen state energy E_i of the unperturbed ($W_{(l)}(r) = 0$) supercell system. Here, we will solve the Eq(6) directly using the conjugate gradient method. The approach is very similar to the method used in perturbation linear response theory [11].

Notice that, the linear equation (6) can be rewritten as an optimization of the following F:

$$F = \langle \psi_{(l)} | H - E | \psi_{(l)} \rangle - \langle \psi_{(l)} | W_{(l)} \rangle - \langle W_{(l)} | \psi_{(l)} \rangle . \quad (7)$$

Preconditioned conjugate gradient method can be used to solve the minimum of F. Unfortunately, for an arbitrary E , the matrix $H - E$ in the above equation is not positive definite, which makes the conjugate gradient method diverges. However, this problem can

be circumvented if we have the eigenstates $\{\psi_i, E_i\}$ of the unperturbed Hamiltonian H . First, if we know all the eigenstates $\{\psi_i, E_i\}$ of H , the $\psi_{(l)}$ in Eq(6) can be solved directly as:

$$\psi_{(l)} = \sum_i^{\infty} \frac{\langle \psi_i | W_{(l)} \rangle}{E_i - E} \psi_i \quad (8)$$

In practice, however, we usually only solve the eigenstates $\{\psi_i, E_i\}$ (using the conjugate gradient method [9]) up to an energy E' (with $E' > \mu_R$). Let's denote this converged set of eigenstates as $i = 1, N$. Then the idea is to deflate these N eigenstates from both $\psi_{(l)}$ and $W_{(l)}$, and solve the remaining part of the wavefunction. More specifically, we can define:

$$\psi_{(l)}^P = \hat{P}\psi_{(l)} = \psi_{(l)} - \sum_{i=1}^N \langle \psi_i | \psi_{(l)} \rangle \psi_i \quad (9)$$

and

$$W_{(l)}^P = \hat{P}W_{(l)} = W_{(l)} - \sum_{i=1}^N \langle \psi_i | W_{(l)} \rangle \psi_i. \quad (10)$$

Then the linear equation

$$(H - E)\psi_{(l)}^P(r) = W_{(l)}^P(r), \quad (11)$$

in the subspace of projector \hat{P} can be solved as the minimum of

$$F^P = \langle \psi_{(l)}^P | H - E | \psi_{(l)}^P \rangle - \langle \psi_{(l)}^P | W_{(l)}^P \rangle - \langle W_{(l)}^P | \psi_{(l)}^P \rangle. \quad (12)$$

Note that, now the effective matrix $\hat{P}(H - E)\hat{P}$ is positive definite as long as E is lower than E_N . When using conjugate gradient method to solve Eq(12), the projector \hat{P} are repeatedly applied to the wavefunctions and search directions, so that the whole minimization is done within the subspace defined by \hat{P} . After $\psi_{(l)}^P$ is solved, $\psi_{(l)}$ of Eq(6) can be obtained from Eqs(9) and (8) as:

$$\psi_{(l)} = \psi_{(l)}^P + \sum_{i=1}^N \frac{\langle \psi_i | W_{(l)} \rangle}{E_i - E} \psi_i. \quad (13)$$

The convergence of $\psi_{(l)}^P$ under the conjugate gradient method is very fast since the effective band gap for $\psi_{(l)}^P$ is $E_N - E$. Kinetic energy G-space diagonal preconditioning can be used, just as in the conventional ground state conjugate gradient method[9]. Fig.2 shows a typical convergence for a $\psi_{(l)}^P$ state. It shows that 20 conjugate gradient line minimizations is enough

to converge the $\psi_{(l)}^P$ to 10^{-6} (a.u.) starting from zero. The $\psi_{(l)}^P$ can be converged to the same accuracy as that of $\{\psi_i, E_i\}$. We find similar convergence for all $W_{(l)}$ and E .

To linearly combine $\psi_{(l)}$ to generate ψ_{sc} of Eq(3), we want to have linearly independent $\psi_{(l)}$. According to Eq(8), if M $W_{(l)}$ are linearly independent, then the corresponding M $\psi_{(l)}$ are also linearly independent. As in Ref. 8, we intend to use the Γ point electrode states as $W_{(l)}$. However, if one or few E_i are very close to E , then their corresponding ψ_i terms might dominate the expression in Eq(8), which can make the $\psi_{(l)}$ lie in similar directions for different l . To avoid this situation, we have modified $W_{(l)}$ as following. Let's use $W_{(l)}^0$ to denote the Γ point electrode states in real space and here l is an index for different bands. $W_{(l)}^0$ are only nonzero at the last primary cell of the right electrode as shown in Fig.1. Then from $W_{(l)}^0$, we can generate $W_{(l)}$ using the following iterations from $\mu = 1$ to $\mu = l - 1$:

$$W_{(l),\mu+1} = W_{(l),\mu} - W_{(\mu)} \frac{\langle \psi_{m_\mu} | W_{(l),\mu} \rangle}{\langle \psi_{m_\mu} | W_{(\mu)} \rangle} \quad (14)$$

and $W_{(l),1} = W_{(l)}^0$ and $W_{(l)} = W_{(l),l}$. In the above equation, m_μ is the i which gives the maximum $|\langle \psi_i | W_{(\mu)} \rangle| / (E_i - E)$ for a given μ . Note that, it is easy to show from Eq(14) that $\langle \psi_{m_\mu} | W_{(l)} \rangle = 0$ for all the $\mu < l$. In other words, $\psi_{(l)}$ as described in Eq(8) [or Eq(13)] will not have the ψ_i component if ψ_i is a maximum component in one $\psi_{(\mu)}$ with $\mu < l$. This makes $\psi_{(l)}$ and $\psi_{(\mu)}$ ($\mu < l$) unlikely to lie in very close directions. Note that $W_{(l)}$ from Eq(14) will still only be nonzero in the last primary cell of the right electrode.

After the M $\psi_{(l)}$ of Eq(6) are calculated following the above procedure for a given E , we will combine these $\psi_{(l)}$ to generate the scattering states ψ_{sc} of Eqs(2),(3). This part is similar to what we have done in Ref. 8. However, more details will be provided here. A band structure alignment between the right and left electrodes is illustrated in Fig.3 with an 4 V bias. The numbers in the right electrode band structure are the index of the electrode bands. In our calculation, we have over cautiously used 11 bands as $W_{(l)}$ in Eq(6). As a result, for a given energy E , we will have 11 $\psi_{(l)}$. Since $\psi_{(l)}^*$ (which has a $-\mathbf{K}_z$ instead of \mathbf{K}_z) also satisfy Eq(6), we end up having 22 wavefunctions to be used in the linear combination to generate ψ_{sc} [in the following, we will denote all these 22 wavefunctions as $\psi_{(l)}$, with $l = 1, M$ and M being 22]. As described in Ref. 8, we will first decompose each $\psi_{(l)}$ at left and right electrode primary cells Ω_L and Ω_R by the electrode wavefunctions. As shown in Fig.3, for a given energy E , we can find the corresponding $k_n^L(E)$ and $k_n^R(E)$ (the small

black dots in Fig.3 on the dashed line E). If the numbers of k in the left and right electrodes are N_L and N_R respectively, then there will be $2(N_L + N_R)$ electrode running waves states (counting also the $-k$). Like in Eq(3), let's use $\phi_n^{R(L)}$ and $\psi_n^{R(L)*}$ to denote these electrode running wave states, then the decomposition of $\psi_{(l)}$ can be written as:

$$\psi_{(l)}(r) = \begin{cases} \sum_{n=1}^{N_R} [A_n^R(l)\phi_n^{R*}(r) + B_n^R(l)\phi_n^R(r)] & \text{if } z \in \Omega_R \\ \sum_{n=1}^{N_L} [A_n^L(l)\phi_n^{L*}(r) + B_n^L(l)\phi_n^L(r)] & \text{if } z \in \Omega_L \end{cases} \quad (15)$$

The coefficients A_n^R, B_n^R can be calculated by the overlap matrix $\langle \phi_n^{R(*)} | \phi_m^{R(*)} \rangle$ and the projection matrix $\langle \psi_{(l)} | \phi_n^{R(*)} \rangle$. The same for A_n^L, B_n^L . The electrode wavefunctions $\phi_n(r)$ are pre-calculated at 50 k points. Then the $\phi_n^R(r)$ for a given k_n^R point is obtained vs interpolation.

Now, combining $\psi_{(l)}(r)$ we have the scattering state as:

$$\psi_{sc}(r) = \sum_{l=1}^M C_l \psi_{(l)}(r). \quad (16)$$

Note, $\psi_{sc}(r)$ satisfies the Schrodinger equation (2) in the region where $W_{(l)}(r)$ are zero (away from B in Fig.1). According to Eq(15), we have $\psi_{sc}(r)$ at Ω_R and Ω_L as:

$$\psi_{sc}(r) = \begin{cases} \sum_{n=1}^{N_R} \{ [\sum_{l=1}^M A_n^R(l)C_l] \phi_n^{R*}(r) + [\sum_{l=1}^M B_n^R(l)C_l] \phi_n^R(r) \} & \text{if } z \in \Omega_R \\ \sum_{n=1}^{N_L} \{ [\sum_{l=1}^M A_n^L(l)C_l] \phi_n^{L*}(r) + [\sum_{l=1}^M B_n^L(l)C_l] \phi_n^L(r) \} & \text{if } z \in \Omega_L \end{cases} \quad (17)$$

Comparing this equation with the boundary equation (3), we have the following $N_R + N_L$ linear equations for a scattering state based on a ϕ_m^{R*} incoming wave:

$$\begin{aligned} \sum_{l=1}^M A_n^R(l)C_l &= \delta_{n,m} & \text{for } n = 1, N_R \\ \sum_{l=1}^M B_n^L(l)C_l &= 0 & \text{for } n = 1, N_L \end{aligned} \quad (18)$$

Note that if $M \geq N_R + N_L$ there can be a solution for the above equation. Given the 11 bands we used as $W_{(l)}$ ($M = 22$), we find that this is always true. When $M > N_R + N_L$, Eq(18) is under determined, meaning there are more than one solutions of C_l . In this case, it makes sense to require the minimum of $\sum_{l=1}^M |C_l|^2$ while Eq(18) is satisfied. This linear algebra problem can be solved using standard numerical routines, like the ZGELSS in LAPACK[10].

After Eq(18) is solved, then we will have a scattering wave ψ_{sc} , which satisfies the Schrodinger's equation (2) within the region from Ω_L to Ω_R , and the boundary condition

of Eq(3) at Ω_L and Ω_R . We can discard the ψ_{sc} of Eq(16) for the regions outside Ω_L and Ω_R (near boundary B). Instead, the real scattering state can be extended following the propagations of the nonzero electrode running waves in Eq(17) into negative and positive infinities. As a result, the boundary conditions of Eqs(17),(18) at Ω_R and Ω_L are the same as the boundary conditions of Eq(3) at $z \rightarrow \infty$ and $z \rightarrow -\infty$.

III. THE EVANESCENT STATES

Above discussions are complete if the electrodes are sufficiently long, so there are no evanescent states at Ω_L and Ω_R . In practices, however, we found evanescent states often exist. There are two type of evanescent states. The first type (type I) originates from the molecule and decays out in the electrodes (i.e. $e^{-\kappa z}$ in the right electrode and $e^{\kappa z}$ in the left electrode). The second type (type II) originates from the artificial boundary B in Fig.1, and decays towards the molecule (i.e. $e^{\kappa z}$ in the right electrode and $e^{-\kappa z}$ in the left electrode). While the first type evanescent states could be physical, existing in a scattering state ψ_{sc} , the second type of evanescent states are artificial due to our use of boundary condition and perturbation $W_{(l)}$ near B . If we can calculate the running wave coefficients $A_n^{R(L)}(l)$ and $B_n^{R(L)}(l)$, then even if we ignore the evanescent states in Eq(15), our resulting scattering state ψ_{sc} constructed from Eq(16) and Eq(18) will still be correct. This is because the evanescent states can be added in as additional terms in Eq(17). As we extend our boundary condition from Ω_L and Ω_R to $-\infty$ and ∞ , the first type evanescent states will decay out, and we can simply remove (subtract out) the second type evanescent states without affecting the Schrodinger's Equation (2) (assuming its amplitude near the molecule is sufficiently small). As a result, we will still have a boundary condition as in Eq(3).

However, it is helpful to include the evanescent states in the decomposition Eq(15) for two reasons: (1) To accurately calculate the running wave coefficients $A_n^{R(L)}(l)$ and $B_n^{R(L)}(l)$; (2) In Eq(16), to avoid the case where large artificial second type evanescent states exist and dominate the equation. As a result, they have significant tail amplitudes near the molecule (compared to the running wave amplitudes). If this is true, then these second type evanescent states cannot be simply removed without introducing errors.

To get $A_n^R(l)$ and $B_n^R(l)$ from Eq(15), we have used the overlap matrix $\langle \phi_n^R | \phi_m^R \rangle_{\Omega_R}$, $\langle \phi_n^{R*} | \phi_m^R \rangle_{\Omega_R}$, $\langle \phi_n^{R*} | \phi_m^{R*} \rangle_{\Omega_R}$ and projections $\langle \psi_l | \phi_n^R \rangle_{\Omega_R}$ and $\langle \psi_l | \phi_n^{R*} \rangle_{\Omega_R}$, then

solved the resulting linear equation. Here the subscript Ω_R means the integration is done only within Ω_R . Since the running waves and evanescent states are not orthogonal within Ω_R , then ignoring the evanescent states in Eq(15) will introduce errors in the resulting $A_n^R(l)$ and $B_n^R(l)$. The situation is the same for the left electrode.

The evanescent states are originated from the real k_e points when $dE_n(k)/dk|_{k=k_e} = 0$. Here the subscript e stands for evanescent states. This happens at the Γ and X' points of the electrode band structure as shown in Fig.3, and at the place where two bands anticross each other and form a band gap. At the Γ point, an evanescent state line runs downward starting from a real Γ point band structure energy. At the X' point and other anticrossing points, two evanescent state lines connect the two real k_e points at the opposite edges of an energy gap. A detail description of the complex band structure is given by Chang in Ref. 12. Although calculating the complex band structure is possible [12], it is difficult for a nonlocal pseudopotential Hamiltonian as is used here. As a result, we have used the real k_e point Bloch states $\phi_{n,e}(r) = u_{n,k_e} \exp(ik_e z)$ to approximate the evanescent states. Notice that, these are just normal running wave states, except that they carry no current since $dE_n(k)/dk|_{k=k_e} = 0$. A more accurate approximation is to add an exponential decaying factor $\exp(\kappa z)$ or $\exp(-\kappa z)$ to $\phi_{n,e}(r)$. However, since we are only going to use $\phi_{n,e}(r)$ within Ω_R or Ω_L , and the surviving evanescent states within Ω_R or Ω_L should have a small κ , we found it is okay for not using these decaying factors. By not adding this decaying factors, we also do not distinguish the type one and type two evanescent states.

Unlike the running wave states whose number is finite for a given energy E , there can be many (actually infinite if we have an infinite basis set) evanescent states for a given E . This is because at the Γ point of the band structure, every new band will have an evanescent state line running downward in energy [12]. As a result, in Eq(15), we cannot include all the possible evanescent states $\phi_{n,e}(r) = u_{n,k_e} \exp(ik_e z)$ for a given E . On the other hand, in practice, it is not necessary to include the evanescent states which are originated from running wave energies $E_n(k_e)$ which are far away from E , because they will have fast decay factors $\exp(\kappa z)$, thus should not exist in Ω_L or Ω_R . Because of this, we have the following practical procedure in solving Eq(15) and selectively including the evanescent states (we will use the right electrode as the example, the same is true for the left electrode): (1) We will start with all the running wave states, calculate the overlap matrix elements $\langle \phi_n^R | \phi_m^R \rangle_{\Omega_R}$, $\langle \phi_n^{R*} | \phi_m^R \rangle_{\Omega_R}$, $\langle \phi_n^{R*} | \phi_m^{R*} \rangle_{\Omega_R}$ and projections $\langle \psi_l | \phi_n^R \rangle_{\Omega_R}$, then solve the linear equations

for $A_n^R(l)$, $B_n^R(l)$. (2) We will calculate the integral of wavefunction square of the right and left hand sides of Eq(15) within Ω_R , and calculate the percentage of the right hand side vs the left hand side results. We will call this decomposition percentage (which is always less than 1). If this percentage is close to 1 within a criterion (e.g., 10^{-4}), then stop. Otherwise go to next step. (3) We will include the next evanescent state which has its $E_n(k_e)$ closest to E . We will include $\phi_{n,e}(r) = u_{n,k_e} \exp(ik_e z)$ in summation of Eq(15), just treat it as one of the running wave states (but if k_e is Γ or X' , $\phi_{n,e}^*(r)$ is the same as $\phi_{n,e}(r)$, thus should not be included). Then repeat step (1),(2), find the new $A_n^R(l)$, $B_n^R(l)$, also the values for the evanescent states $A_{n,e}^R(l)$, $B_{n,e}^R(l)$. If one evanescent state has almost zero (e.g., less than 10^{-4}) contributions in all $\psi_{(l)}(r)$, then discard this evanescent state. If the decomposition percentage is still not close enough to 1, repeat step (3). If the total number of evanescent state is too big (e.g, larger than 10), or the next closest $E_n(k_e)$ is too far away from E (e.g, farther than 2 eV), then stop.

Let's assume that through the above procedure, we have included N_L^e , N_R^e evanescent states (counting both possible $\phi_{n,e}$ and $\phi_{n,e}^*$) to the Ω_L and Ω_R sub-equations in Eq(15). If we have $M > N_R + N_L + N_R^e + N_L^e$ (situation I), then we can request all the evanescent state coefficients to be zero after the linear combination in Eq(17) [e.g, $\sum_{l=1}^M A_{n,e}^{R(L)}(l)C_l = 0$, $\sum_{l=1}^M B_{n,e}^{R(L)}(l)C_l = 0$]. These are $N_L^e + N_R^e$ additional equations to Eq(18). Since we still have more number of C_l than the total number of linear equations, we can still request the $\sum_{l=1}^M |C_l|^2/\omega_l$ to be minimum while these equations are satisfied (again, this can be solved by the ZGELSS LAPACK routine [10]). Here we have placed a weight function ω_l , which depends on the decomposition percentage (after the inclusion of the evanescent states) of each $\psi_{(l)}$ in Eq(15). If the decomposition percentage is close to 1 [a good fit in Eq(15)], then ω_l is close to 1. If the decomposition percentage is much less than 1 [not a very good fit in Eq(15)], then ω_l is very small, which means $\psi_{(l)}$ is discouraged from participating in the linear combination of Eq(16). More specifically, if we use p_l^R and p_l^L to denote the decomposition percentage of the $\psi_{(l)}$ at Ω_R and Ω_L in Eq(15), then we have used a formula $\omega_l = 0.001/(0.001 + |p_l^R - 1|) + 0.001/(0.001 + |p_l^L - 1|)$. In another situation (situation II), we have $N_R + N_L \leq M \leq N_R + N_L + N_R^e + N_L^e$. Then to solve C_l , we can minimize the evanescent state coefficients after the linear combination of Eq(16) [i.e, minimize $\sum_{n,R,L} |\sum_{l=1}^M A_{n,e}^{R(L)}(l)C_l|^2 + |\sum_{l=1}^M B_{n,e}^{R(L)}(l)C_l|^2$] while satisfying Eq(18) exactly. This again can be solved by standard numerical packages. In our calculation, we find all of

our cases fall into situation I.

In the situation I, we have requested the evanescent state coefficients in the scattering state of Eq(16) to be zero. This might look strange at first. As we discussed above, the type I evanescent state might be physical in a scattering state. Then, how can we force it to be zero and still have a good scattering state? The answer lies in the fact that we did not separate the evanescence state $\phi_{n,e}(r) = u_{n,k_e} \exp(ik_e z)$ into the type I and type II states [i.e., $\phi_{n,e} e^{\kappa z}$ and $\phi_{n,e} e^{-\kappa z}$]. As a result, the coefficient we have for $\phi_{n,e}(r)$ is really the sum of the coefficients for the type I and type II states. As a result, in a scattering state ψ_{sc} , although we cannot force the coefficients of type I evanescent states to be zero, we can always add a type II states to cancel their coefficients. So, when we require the coefficients of $\phi_{n,e}(r)$ to be zero, it doesn't mean the type I evanescent state coefficients are zero. However, since the possible type I evanescent state coefficient in a given scattering state ψ_{sc} is fixed and is likely small at Ω_L and Ω_R , then our type II evanescent state coefficient should also be small. This guarantees that the erroneous situation of large type II evanescent states (as we discussed near the beginning of this section) will never happen, and our results are always stable and accurate.

IV. THE RESULTS

Following the above procedures, we have calculated the system in Fig.1 with different biases. We have compared the current results with the results reported in Ref. 8. First, using the conventional ground state conjugate gradient program [13], we have solved all the eigen states of H up to ~ 0.5 eV above the right electrode Fermi energy μ_R . In our system, this amounts to ~ 140 eigen states. Then we have scanned the scattering state energy E with an interval of ~ 0.04 eV. For each l and E , as shown in Fig.2, Eq(11) of $\psi_{(l)}^P$ can be solved by the conjugate gradient method within 20 line minimizations up to 10^{-6} a.u. accuracy. Next, decomposition of $\psi_{(l)}$ is carried out at Ω_R and Ω_L as described by Eq(15) including the evanescent states. We find that, for most $\psi_{(l)}$, the running wave alone can get a decomposition percentage up to 99.999% or higher. However, for each energy E , it is very likely that there are one or two $\psi_{(l)}$ with their running wave decomposition percentage only up to 50% or smaller. It is also likely that, even after including the approximated evanescent states, there are still one or two $\psi_{(l)}$ with their decomposition percentage only

being around 90%. However, since these $\psi_{(l)}$ have very small ω_l in the minimization of $\sum_l^M |C_l|^2/\omega_l$, their C_l are often exceedingly small (e.g, $< 10^{-10}$) in the linear combination of Eq(15). Following the procedure described above, a scattering state ψ_{sc} of Eqs(16),(17),(18) is solved for each right electrode running wave ϕ_m^{R*} . The typical ψ_{sc} wavefunctions look the same as illustrated in Fig.3 of Ref. 8. The transmission coefficient $T_m(E)$ is calculated for the scattering state according to Eq(4). We find that the current conservation equation (5) is mostly satisfied beyond 99.9%, and in many cases beyond 99.999%, an indication of the numerical accuracy of this approach. However, there are occasional and distinctive cases where Eq(5) is not satisfied at all (e.g., the sum of transmission and reflection is 10^5 , instead of 1). In these cases, the evanescent states in the constructed scattering state of Eq(16) are not eliminated, but dominating, perhaps due to our approximations in the treatment of the evanescent states. Fortunately, these cases are very rare and can be easily detected, thus to be discarded.

Figure 4 shows the calculated transmission coefficients $T_n(E)$ for different band n , plotted as functions of the k_z points. The system has a bias of 4V. Each cross symbol corresponds to a calculated scattering state ψ_{sc} . We have also plotted the calculated $T_n(E)$ using our previous method [8] as rectangular symbols. As we can see, the current method and the previous method yield the same T_n amplitudes. This is a cross check for the robustness of these two methods. However, since the E in the previous method can only be the eigen energies E_i of the original H , it only yields a finite number of the scattering states. In contrast, the current method can have as many scattering states as we want. Actually, as shown in Fig.4, there are cases (e.g, for $n = 5$ and for the dip near $k_z = 0.9\pi/a$ of $n = 1$) where the previous method might not have enough calculated points to reveal the sillenXX nature of the $T_n(k_z)$ curve. In terms of the computational time, we find the current method is faster than the previous method, despite the fact that we now have much more data points. We find that for the number of E points we used, the total time spent to solve Eq(11) for all the energies and l is about 2 times the time spent to solve all the ground states ψ_i of the original Hamiltonian H . This makes our transport computational time in the same order as a typical ground state calculation.

The points in Fig.4 are fitted by smooth curves $T_n(k_z)$ as described in Ref. 8, and the resulting curves are used to plot the total transmission coefficients $T(E) = \sum_n T_n(k_z(E))$, which is shown in Fig.5. Again, we have compared our current results with our previous

results [8] for the biases of 1 V and 4 V cases. We see that, overall, they are almost the same. But there are some differences in the detail. In the bias 1 V case, near $E - E_F = -1.5$ eV, the current method produce a well shape dip. This is due to a gap at the X' point of the left electrode near $E - \mu_L = -0.5$ eV. The previous method missed this dip because it doesn't have a data point with its energy falls into this left electrode energy gap. In the bias 4 V case, near $E - E_F = 0$ eV, the current $T(E)$ is lower than the previous results. This is because in the $n = 5$ band of Fig.4, the previous method has only two points at the $k_z < 0.6\pi/a$ region. This leads to a fitted $T_n(k_z)$ which is too high compared to the correct result, and consequently an over estimated $T(E)$ near $E - E_F = 0$.

Despite the above differences between the current $T(E)$ and the previous results, their calculated total currents are very similar. For example, in the cases of 1 V and 4 V biases, the current method produces currents 0.0390 and 0.376 e^2V/h respectively, while the previous method produces 0.0417 and 0.398 e^2V/h respectively. The differences are only about 5%. The I-V curve produced by the current method is very close to the result of the previous method, which is shown in Fig.6 of Ref.8.

V. CONCLUSION

In conclusion, we have presented a new approach to calculate the quantum transports. The current method is based on a previous method [8] which uses the periodic boundary conditions, thus makes it possible to use the popular pseudopotentials and planewave basis set. Compared to the previous method [8], however, the current method uses a different way to solve the periodic wavefunction $\psi_{(l)}$ of Eq(6). As a result, the scattering states can be calculated at any given energy E . This provides a more robust way to calculate the scattering state wavefunctions and their transmission coefficients. Under the current method, the total computational time for a transport problem is in the same order as the computational time of its corresponding ground state problem. Enough details of the procedure is presented which makes the implementation of this method possible.

Acknowledgments

This work was supported by U.S. Department of Energy under Contract No. DE-AC03-76SF00098. This research used the resources of the National Energy Research Scientific Computing Center at Lawrence Berkeley National Laboratory.

- [1] J. Taylor, H. Guo, J. Wang, Phys. Rev. B **63**, 245407 (2001); P. Damle, A. Ghosh, S. Datta, Phys. Rev. B **64**, 201403 (2001); M. B. Nardelli, J.-L. Fattebert, J. Bernholc, Phys. Rev. B **64**, 245423 (2001); M. Brandbyge, *et.al*, Phys. Rev. B **65**, 165401 (2002); E. Louis, *et.al*, Phys. Rev. B **67**, 155321 (2003).
- [2] K. Hiros, M. Tsukada, Phys. Rev. B **51**, 5278 (1994);
- [3] H.J. Choi, J. Ihm, Phys. Rev. B **59**, 2267 (1999).
- [4] D. Z.-Y. Ting, E. T. Yu, T.C. McGillha, Phys. Rev. B **45**, 3583 (1992).
- [5] M. Di Ventura, S.T. Pentelides, N. D. Lang, Phys. Rev. Lett. **84**, 979 (2000); M. Di Ventura, N. D. Lang, Phys. Rev. B **65**, 45402 (2001).
- [6] M.A. Reed, *et.al*, Science **278**, 252 (1997).
- [7] P.W. Chiu, M. Kaempgen, and S. Roth, Phys. Rev. Lett. **92**, 246802 (2004).
- [8] L.W. Wang, //arxiv.org/abs/cond-mat/0408222
- [9] M.C. Payne, M.P. Teter, D.C. Allan, T.A. Arias, and J.D. Joannopoulos, Rev. Mod. Phys. **64**, 1045 (1992).
- [10] E. Anderson, *et. al.*, *LAPACK User's Guide, Third Edition* (SIAM, Philadelphia, 1999).
- [11] X. Gonze, Phys. Rev. B **55**, 10337 (1997).
- [12] Y.C. Chang, Phys. Rev. B **25**, 605 (1982).
- [13] <http://crd.lbl.gov/~linwang/PEtot/PEtot.html>

FIG. 1: A schematic view of the calculated system.

FIG. 2: The conjugate gradient (CG) convergence of Eq(11). The convergence error is defined as $\| (H - E)\psi_{(l)}^P - W_{(l)}^P \|$.

FIG. 3: The band alignment between the left electrode band structure and the right electrode band structure. The voltage bias is 4 V. The numbers in the right electrode band structure are the band index. The small black dots on the line E are the k_n^L and k_n^R points satisfying $E_n^L(k_n^L) = E$ and $E_n^R(k_n^R) = E$ respectively.

FIG. 4: The calculated transmission coefficients $T_n(k_n^R)$. The crosses are the results from the current method, the rectangulars are the results from the previous method Ref. 8, and the lines are the fitted smooth curves for the current results.

FIG. 5: The calculated total transmission coefficients $T(E)$ for different biases. The zero is the right electrode Fermi energy. For a given bias V, there are net right to left current flow only within the $[-V, 0]$ energy window.

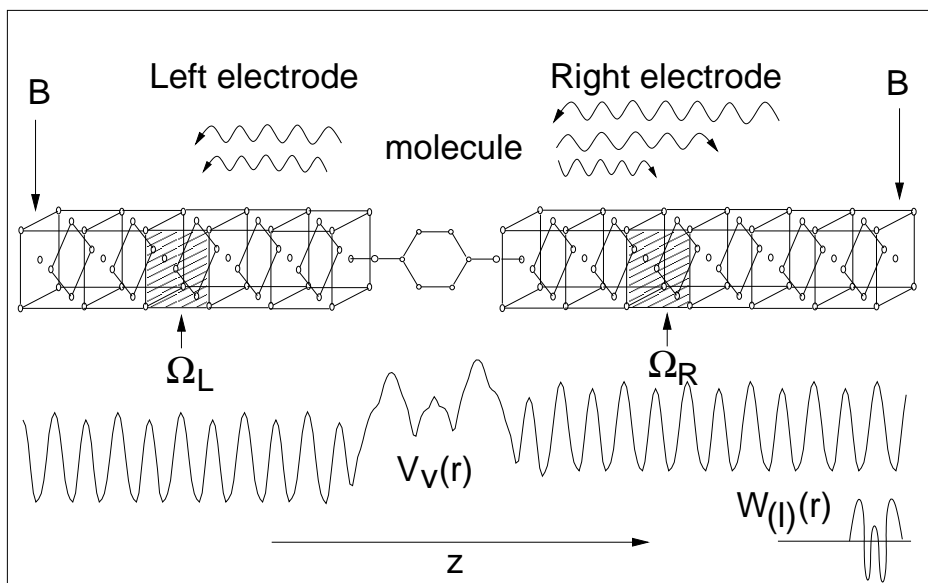


Fig.1, Wang

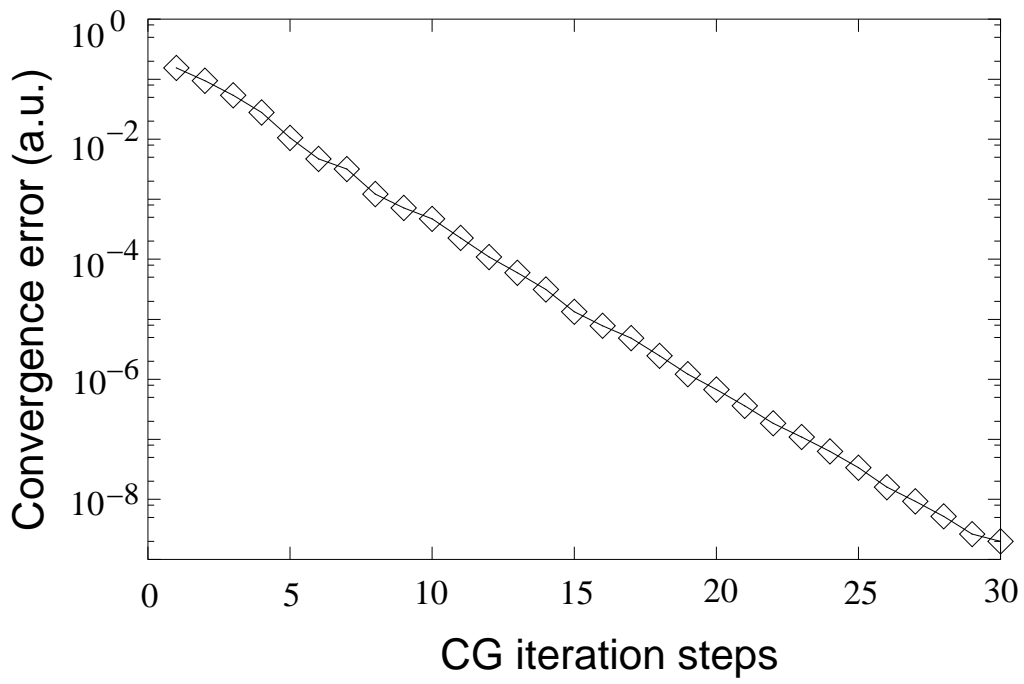


Fig.2, Wang

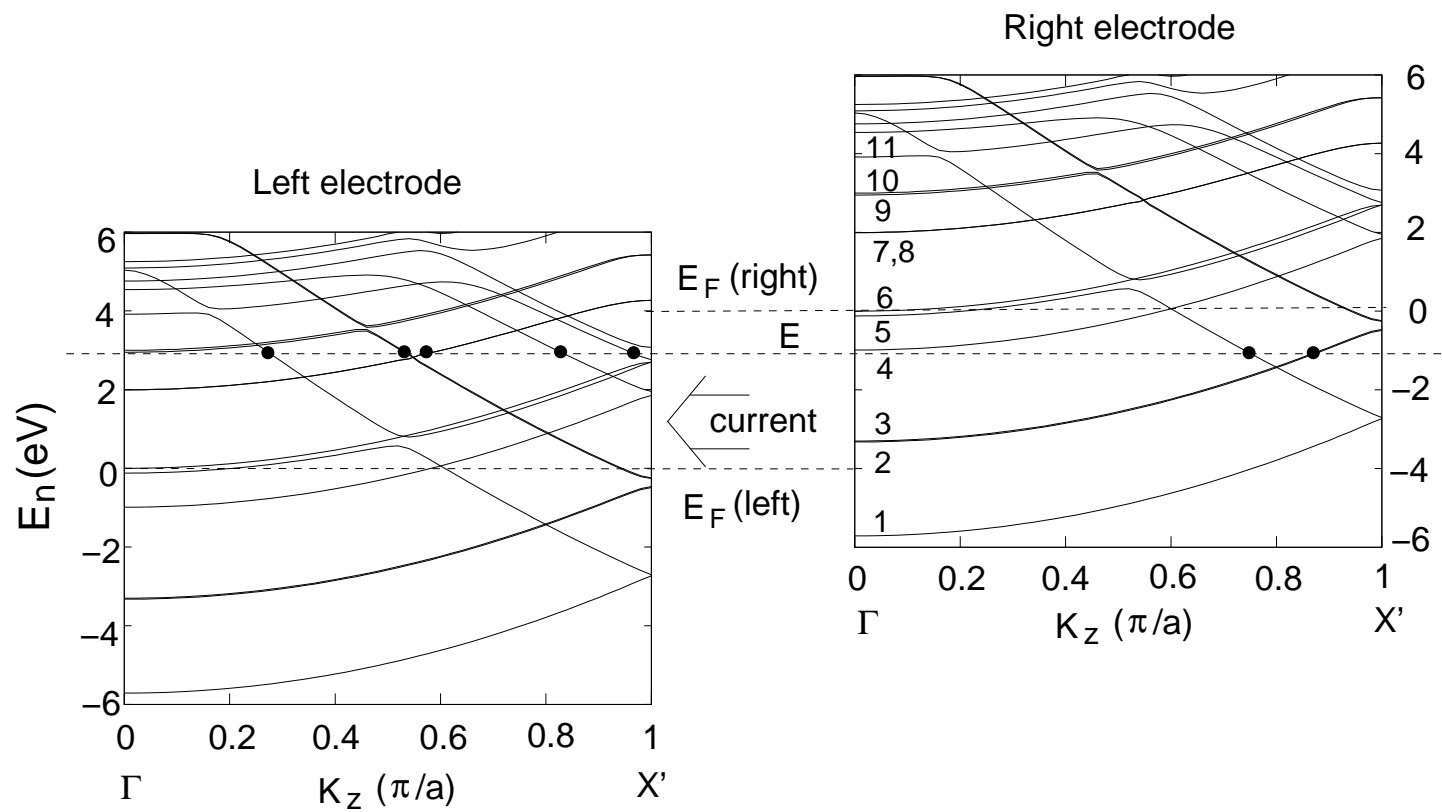


Fig.3, Wang

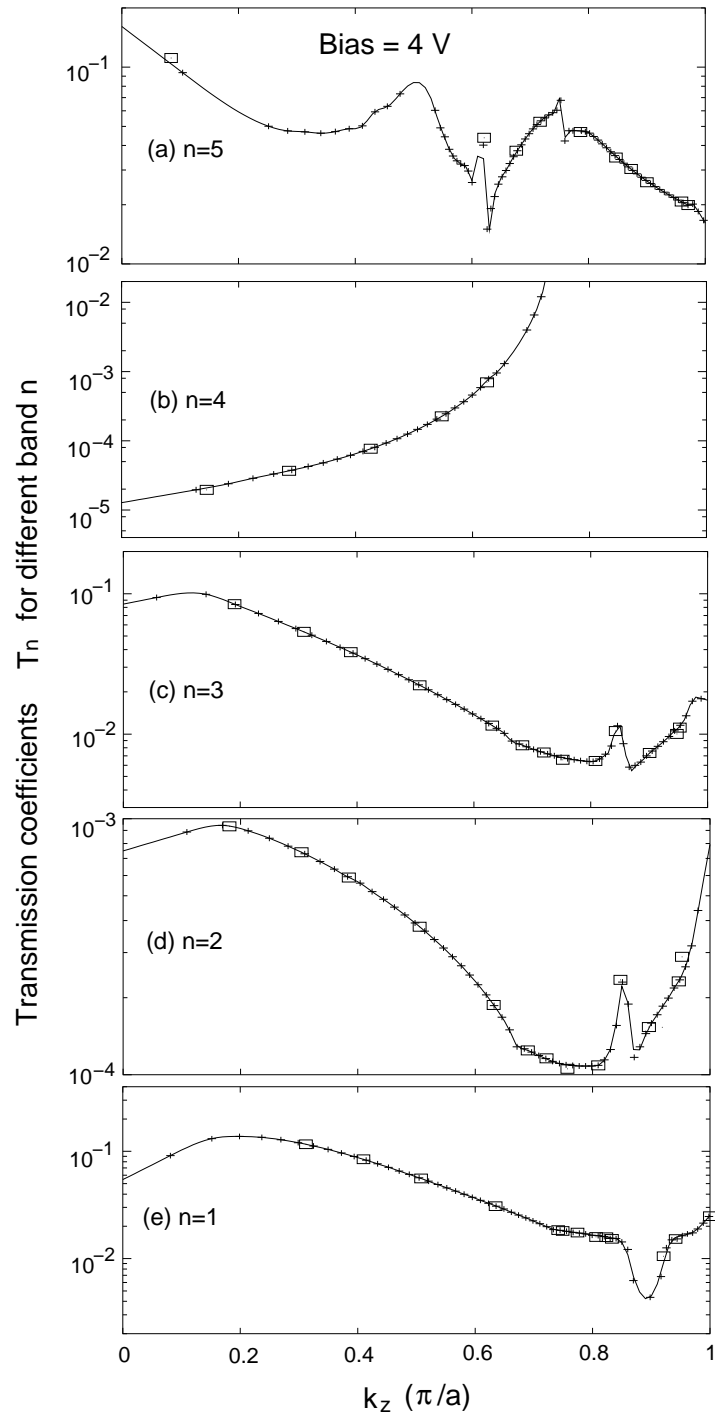


Fig.4, Wang

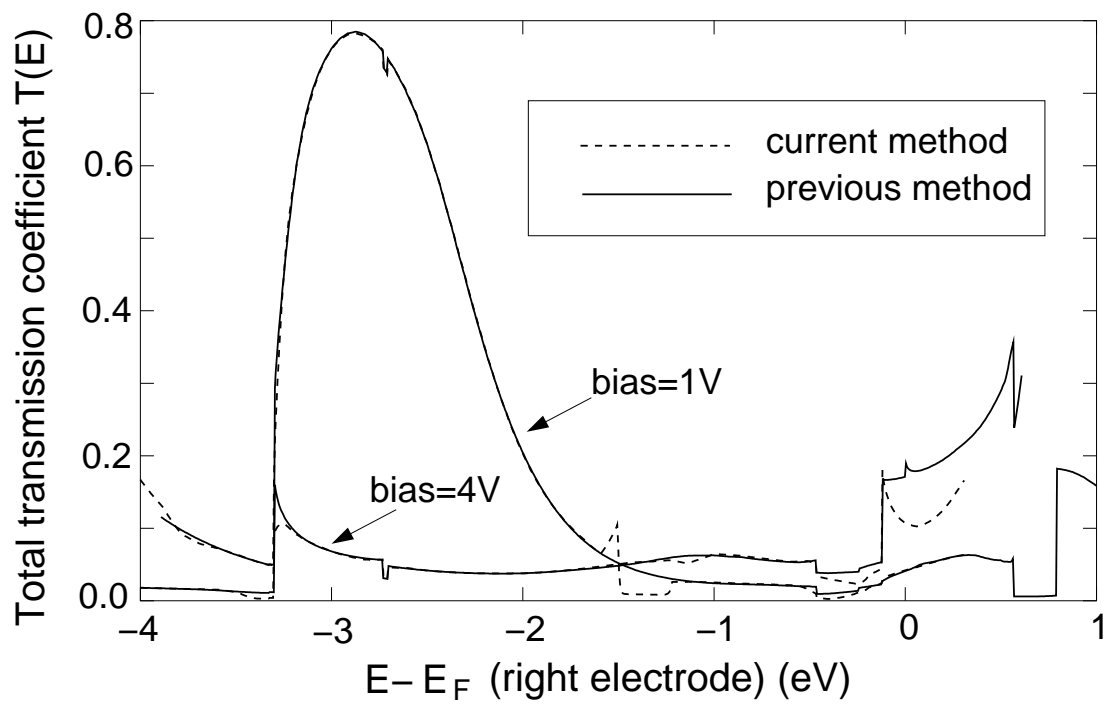


Fig.5, Wang